Invited Paper

Ultrafast carrier dynamics in graphene and graphene nanostructures

Dmitry Turchinovich [1*], Zoltan Mics [1], Søren A. Jensen [1], Klaas-Jan Tielrooij [1, 2], Ivan Ivanov [1], Khaled Parvez [1], Akimitsu Narita [1], Tobias Hertel [3], Frank Koppens [2], Xinliang Feng [1], Klaus Müllen [1], and Mischa Bonn [1]
[1] Max Planck Institute for Polymer Research, Ackermannweg 10, 55128 Mainz, Germany
[2] ICFO – Institut de Ciencies Fotoniques, Mediterranean Technology Park, Castelldefels, Barcelona, 08860 Spain
[3] Institute of Physical and Theoretical Chemistry, Julius-Maximilian University, 97070 Würzburg, Germany
[*1] Email: turchino@mpip-mainz.mpg.de

(Received December 14, 2015)

Abstract: In this paper we provide a comprehensive view on the ultrafast conduction dynamics in graphene and graphene nanostructures. We show that ultrafast conduction in graphene can be well understood within a simple thermodynamic picture, by taking into account the dynamical interplay between electron heating and cooling, with the driving electric field acting as a supplier of thermal energy to graphene electron population. At the same time, the conductive properties of graphene nanostructures, such as graphene nanoribbons (GNRs) and carbon nanotubes (CNTs), can be well explained within the concept typical for disordered materials, such as e.g. organic semiconductors - the conduction by the free charge experiencing long-range localization.

Keywords: Terahertz spectroscopy, Graphene, Nanostructures, Conductivity, Charge transport properties.

doi: 10.1051/tst/2020134135

1. Introduction

Owing to its outstanding electrical and thermal properties, graphene is considered extremely promising for high-speed electronics [1]. In graphene, free charge carriers within the Dirac cone behave like massless fermions with a very high group velocity, the Fermi velocity, only ~300 *times* lower than the speed of light in vacuum [2]. The field effect in graphene, i.e. the change in conductivity induced by an externally applied gate potential, which is crucial for transistor operation, was demonstrated in 2004 [3, 4]. A graphene transistor operating at the frequency as high as ~400 *GHz* was recently demonstrated [5], and the ambition in the industry is to reach the terahertz (THz) operation regime.

In this paper we present a comprehensive picture of ultrafast conduction of graphene, which shows that intrinsic conductivity of graphene under high-frequency modulation is in fact radically different from that observed in static conditions. Our experiments, supported by a simple

thermodynamic model, reveal that the high-frequency electron transport in graphene is governed by a remarkably efficient intra-band carrier heating by strong THz fields. The thermodynamic model not requiring any knowledge of microscopic electron kinetics, perfectly well describes the entirety of our experimental data on THz conductivity of graphene, which also includes the THz photoconductivity.

Further, we discuss the photoconductivity in graphene nanostructures such as graphene nanoribbons (GNRa) and carbon nanotubes (CNTs), which is governed by the laws typical for disordered materials, such as e.g. organic semiconductors - the conduction by the free charge experiencing long-range localization.

2. Sample

Our monolayer-thick graphene sample is grown on copper by chemical vapor deposition (CVD) [6] and is transferred onto a fused silica substrate, which introduces *p*-doping [7, 8]. We characterize the sample using steady-state THz [8] and Raman [9, 10] spectroscopy. We determine the position of the Fermi energy to be $E_F = 0.07 \pm 0.01$ *eV* with respect to the Dirac point, corresponding to a sheet carrier density of $N_s = (6.0 \pm 2.0) \times 10^{11}$ cm^{-2}. The negligible D peak in the Raman spectrum demonstrates high sample quality, which is confirmed by the electron momentum scattering time of 140 *fs* corresponding to a mean free path of 140 *nm*, and a dc mobility of 13,000 cm^2/Vs. This makes our sample comparable to the highest quality CVD graphene samples described in the literature [8, 11-13]. The details of sample preparation, initial characterization, and comparison with the state-of-the-art can be found in [14]. For simplicity, and given the full symmetry of the valence and the conduction bands in graphene, we refer here to the free charges as electrons, and depict the Fermi level in the conduction band instead of the valence band.

3. Nonlinear THz spectroscopy – intrinsic carrier response in graphene to THz fields

To investigate the high-field, high-frequency conductive properties of graphene under conditions typical for high-speed MOSFETs (field strength of~100 *kV/cm*, modulation frequency ~ 1 *THz*), we perform frequency-resolved and contact-free I-V characterization, using an all-optical method called nonlinear ultrafast THz spectroscopy [15]. This method is based on the principle depicted in Fig. 1(a): a freely propagating, single-cycle, sub-picosecond transient of THz radiation is transmitted through the material of interest.

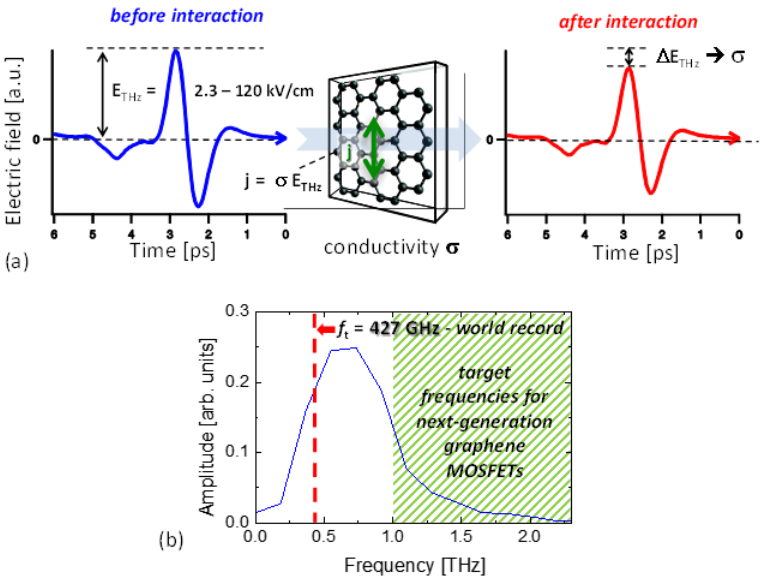

Fig. 1 Schematic of the ultrafast I-V measurement. (a) Oscillating THz probe with controllable peak field E_{THz} incident from free space, induces the time-dependent current in graphene $j = \sigma E_{THz}$, which leads to the attenuation of the THz probe field ΔE_{THz} due to the conductivity of graphene σ. The Fourier transforms of the THz probes measured before and after the interaction with graphene yield its frequency-dependent conductivity. Thus, the conductivity of graphene is determined for all the frequencies contained in the single-cycle THz probe, the amplitude spectrum (b) of which is covering the operation frequency range of both current and next-generation MOSFETs. The experiment in (a) is repeated for several values of the THz peak field strength in the range 2.3-120 *kV/cm*, yielding the ultrafast and contact-free I-V characterization of graphene – its frequency- and peak field- dependent conductivity spectrum.

The time-dependent electric field of the incident signal E_{THz} induces the current $j = \sigma E_{THz}$ in graphene, proportional to its conductivity σ. The generation of this current leads to the attenuation of the electric field of the THz pulse, as it is transmitted through the sample. Due to its single-cycle nature, the THz waveform used in the measurements has a broad frequency spectrum, as shown in Fig. 1(b). The THz signals before and after the interaction with the sample are recorded in the time domain. The analysis of the incident and transmitted pulses is performed in the frequency domain: Fourier transforms of the time traces yield the ac conductivity spectrum of the probed material in the THz frequency range [15, 16]. The key advantage of this all-optical method is that the *intrinsic* high-frequency conductivity of materials can be accessed in a non-contact fashion, that is, without any external circuitry. The inherently broad frequency content of terahertz pulses, along with the ability to tune the peak field strength up to several hundreds of kV/cm [17, 18] allows us to determine the frequency-and field strength-dependent response of the material [13, 15, 19-22]. Applying this method, we present a high-frequency I-V characterization of graphene under electrical modulation with peak fields in the range 2.3-120 *kV/cm*, and in the frequency range 0.3-1.2 *THz*, covering both the sub-THz operation frequencies of the current generation of graphene transistors, and the target operation frequencies of future-generation devices exceeding 1 *THz* [23] (see Fig. 1). All our measurements are carried out at room temperature.

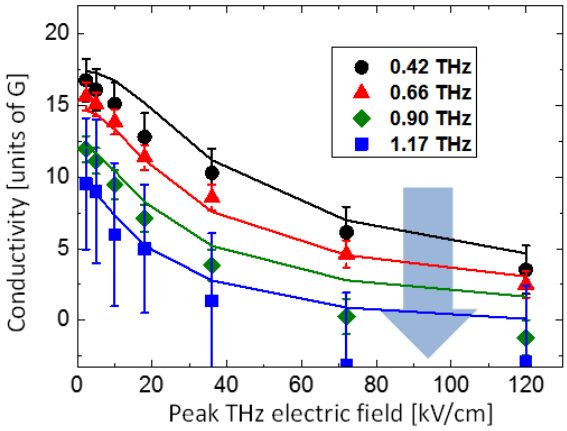

Fig. 2 Reduction of graphene conductivity with increase in modulation frequency and field strength. Symbols – measured real-valued conductivity of graphene as function of THz field strength and THz frequency. Lines – model based on carrier heating as explained in the text. The conductivity is expressed in quantum units of G = $e^2/4\hbar$. The blue arrow illustrates the trend in conductivity reduction with increase in driving field frequency.

Figure 2 shows our key observation: the dependency of the (real-valued) graphene conductivity on the peak of the applied electric field, measured at different frequencies in the range 0.4-1.2 *THz*. Clearly, the conductivity of THz-modulated graphene decreases dramatically both with increasing peak modulation field strength and frequency. At the highest frequency and field strength (1.17 *THz* and 120 *kV/cm*), the conductivity of graphene vanishes almost completely, whereas at the lowest frequency (0.4 *THz*), the conductivity decreases by a factor of five, from 17 *G* down to 3.5 *G*, as the THz field strength increases from 2.3 *kV/cm* to 120 *kV/cm*. Here G = $e^2/4\hbar$ = 6.04 $\times 10^{-5}$ S is the quantum conductivity unit [24], e is elementary charge, and $\hbar = h/2\pi$ is the reduced Planck's constant).

We will show that the observed suppression of the graphene conductivity under strong THz electrical modulation is directly caused by a THz-induced elevation of the electron temperature. Indeed, heating of the electron bath in intrinsically doped graphene as a result of optical, inter-band excitation has previously been shown to result in the reduction of the THz-frequency conductivity [25, 26]. This process is mediated by highly efficient intra-band carrier-carrier scattering leading to ultrafast, sub-50 fs thermalization of the free charge population [27, 28].

The similarity between the suppression of graphene THz-frequency conductivity under inter-band optical excitation [8, 25] and under the intra-band high-field THz conditions observed here, suggests that the electrons acquire considerable amounts of energy from the THz field, which are comparable to the energies received from the photons under optical pumping [8, 25]. The amount of energy per unit area transferred to graphene from the THz modulation signal can be readily obtained from the absorbed terahertz power [20]. We find that as much as ~ 0.05 $\mu J/cm^2$ of energy is transferred to graphene from the THz signal at high field strengths, which is indeed comparable to the energies transferred as a result of intense optical pumping, leading to THz conductivity reduction [8, 25].

4. Thermodynamic approach to graphene THz conductivity

The difference between the inter-band and intra-band excitation of graphene lies in the primary mechanism of interaction between the excitation field and the material. For inter-band excitation [8, 25], photons are directly converted into photo-excited electron-hole pairs. The energy of photoexcited carriers is then primarily transferred to the free carrier bath via efficient electron-electron interaction [25, 29], leading to near-instantaneous thermalization of the electron system. The hot electron distribution in turn relaxes by transferring its energy to the lattice via phonon emission as described in [25, 27, 28]. In case of intra-band excitation of (doped) graphene by the THz field, the energy transfer occurs via the conductivity mechanism – the THz field E_{THz} acts on the free carriers in graphene and drives the THz current $j = \sigma E_{THz}$, and the THz power absorption A of graphene is proportional to its conductivity σ. However, due to extremely efficient electron-electron interaction in graphene, the THz-driven electron population thermalizes on the time-scale which can be considered instantaneous as compared to the oscillation dynamics of THz field. Hence, the THz energy coupled to graphene via the conductivity mechanism is quasi-instantaneously converted into the *thermal* energy of electron population, which can be described by the Fermi-Dirac distribution corresponding to elevated electronic temperature T_{el}. The carrier cooling naturally occurs via the same mechanism as for inter-band excitation, i.e. via the phonon emission [28].

We now quantitatively reproduce the measured THz frequency- and field-dependent conductivity of graphene, based on the above thermodynamic picture. The results are shown as solid lines in Fig. 2, as provided by a simple thermodynamic model presented below. The model describes the THz frequency - dependent conductivity of graphene using the Boltzmann equation with a Fermi-Dirac distribution of carriers characterized by an electron temperature T_{el} and chemical potential μ. We use the following form of the conductivity spectra, directly derived from the Boltzmann equation (see: [30-32]):

$$\sigma(\omega) = -\frac{e^2 {v_F}^2}{2}\int_0^\infty D(E)\frac{\tau(E)}{1-i\omega\tau(E)}\frac{\partial f_{FD}(\mu,T,E)}{\partial E}dE. \quad (1)$$

Here $D(E) = \frac{2}{\pi\hbar^2{v_F}^2}|E|$ is the energy-dependent density of states [32], and $\tau(E)$ is the energy-dependent carrier momentum scattering time. Before the interaction of graphene with the THz field, the carrier distribution is considered cold (i.e. room-temperature) with $\mu\ (300\ K) = E_F = 0.07\ eV$. After the interaction, the temperature is elevated and the carrier distribution is changed as illustrated in Fig. 4(a, b). We account for the heating of the carrier system by simply adding an amount of heat ΔQ (due to the THz field) to the carriers. We apply the laws of conservation of energy: $Q = Q_0 + \Delta Q = \int_0^\infty E\, D(E) f_{FD}(\mu, E)\, dE$, where Q_0 is the thermal energy of the cold carrier distribution at 300 K, and the conservation of conduction band carrier density at all times: $N_s = \int_0^\infty D(E) f_{FD}(\mu, E)\, dE = const$. The latter condition importantly implies that the chemical potential decreases with increasing carrier temperature and

concomitant broadening of the Fermi-Dirac distribution (as a result of the linearly-increasing with energy density of states in graphene D(E)).

This downshift of the chemical potential with increasing electronic temperature, following from the conservation of carrier density, in turn leads to opening up of more inter-band absorption channels with the energy of $> 2\mu$. (which were Pauli-blocked before). Applying the conservation of total spectral weight, we find that opening up more inter-band absorption channels must be compensated by reducing the weight of intra-band absorption, which contributes to the THz conductivity of graphene. As a result, the downshift in chemical potential at higher electronic temperatures provides the qualitative explanation for lower THz conductivity in graphene as stronger fields.

For a quantitative description of the conductivity, the energy dependence of electron scattering time $\tau(E)$ in Eq. (1) needs to be taken into account. As described in detail in [30] and references therein, electron scattering in graphene can occur in two different energy-dependent regimes. The electrons can undergo long-range scattering with Coulomb impurities, where the electron scattering time is proportional to the electron energy $\tau = \gamma E$; and the electrons can undergo short-range disorder scattering with the inverse dependency of scattering time on electron energy $\tau = \beta/E$. The former is the predominant scattering mechanism for a CVD-grown graphene as used in our work [30], whereas the latter is predominant in high quality (encapsulated or suspended) exfoliated graphene [30]. The proportionality constants can be readily obtained experimentally from the linear characterization of graphene, as $\gamma = \tau_0 (300\ K)/ \boldsymbol{E_F}(300\ K)$ $\beta = \tau_0 (300\ K)*\boldsymbol{E_F}(300\ K)$ [14]. However, the argument of the conservation of spectral weight, increasing inter-band conductivity of graphene at higher carrier temperature at the expense of reducing the intra-band (THz) conductivity, demonstrates that the precise knowledge of energy dependency of momentum scattering time in graphene is not essential for predicting the reduction of strong-field THz conductivity in graphene.

Direct application of Eq. 1 to the data in the constraint of energy and carrier density conservation (and assuming the long-range Coulomb momentum scattering mechanism), allows us to very well describe the measurements taken up to the field strength of 40 *kV/cm*, using the effective carrier temperature as free parameter. For the THz field strength of 40 *kV/cm* we therefore can assign the electron temperature of ~1000 *K*, which is close to the value of Fermi temperature of our sample [14]. For the stronger fields, however, the static description by simply using Eq. 1 on the data becomes somewhat inaccurate, calling for the time-dependent treatment of the heat balance in the electronic population of graphene. Using a split-step time-domain approach, and by treating the carrier heating as an instantaneous process, and the carrier cooling occurring via phonon emission as a retarded process with known dynamics [27, 28], we manage to reproduce the whole entirety of our data, taken at all field strengths 2.3-120 *kV/cm*, and in the entire frequency range up to 1.2 *THz*, without using any effective parameters, as shown in Fig. 3 [14].

As one can see, at the frequencies above 1 *THz*, and the THz peak fields of ~ 100 *kV/cm*, the conductivity of graphene almost entirely vanishes, while the calculations deliver the peak electron temperatures exceeding 7000 *K* for the strongest fields used (a typical MOSFET operation regime) [14]. On the average, comparing the experiments and the data yields the field-strength independent electron heating efficiency of about 15% for the THz pulses used in this measurements (see Fig. 1). That is, on the timescale of graphene-THz interaction of 1.5-2.0 *ps*, about 15% of absorbed THz energy is retained as electronic heat, whereas the rest of it is spent on the emission of phonons.

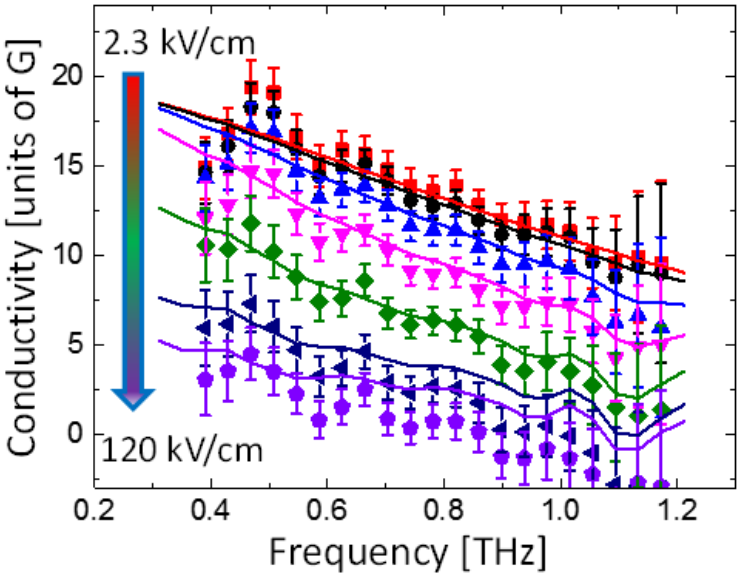

Fig. 3 Measured (symbols) and modelled (lines) conductivity spectra of graphene for the entire range of THz field strengths 2.3-120 *kV/cm*, and for the entire experimental frequency range up to 1.2 *THz*. The increase in the THz field strength leads to monotonous overall reduction of THz conductivity.

5. Optical pump – THz probe spectroscopy of graphene: photoconductivity measurements

Since it was shown that the intrinsic electronic THz conductivity in graphene can be perfectly well understood within a simple yet accurate thermodynamic picture [14] (see also Section 3), we can now apply the same formalism to treatment of the photoconductivity – i.e. the conductivity of graphene under optical illumination, leading to inter-band transitions. It is well known that, unlike in typical semiconductors [16] the photoconductivity of doped graphene is negative, i.e. its conductivity in the presence of photo-excitation decreases (see e.g. [8]). The reason for this is the effective redistribution of energy of pumping photons to the background free electron population, leading to its heating [25]. Now, using the thermodynamic approach [14], the THz photoconductivity of graphene can be easily quantified, and the carrier heating efficiency can be accurately determined based on the established electron temperature [29].

In Fig. 4 the complex-valued photoconductivity spectrum of doped graphene, photoexcited at 800 *nm* is shown (pump-probe delay of ca. 0.5 *ps*). The photoexcitation tends to leading to photo-carrier density of 8×10^{12} cm^{-2}. As is clearly seen in Fig. 4, the real part of the conductivity is negative, which is photoexcitedly doped graphene that indeed loses its THz conductivity in the presence of high-energy, photo-excited carriers. As the solid line in Fig. 4, the result of the fit is shown, which is essentially the difference between two conductivities described by Eq. 1: one of the graphene sample with the carrier temperature Tel = 300 *K* (see also Fig. 3), and one corresponding to a certain elevated carrier temperature acting as a fit parameter [29]. It is apparent from Fig. 4 that the simple thermodynamic model Eq. 1 indeed describes the photoconductivity of graphene just as good.

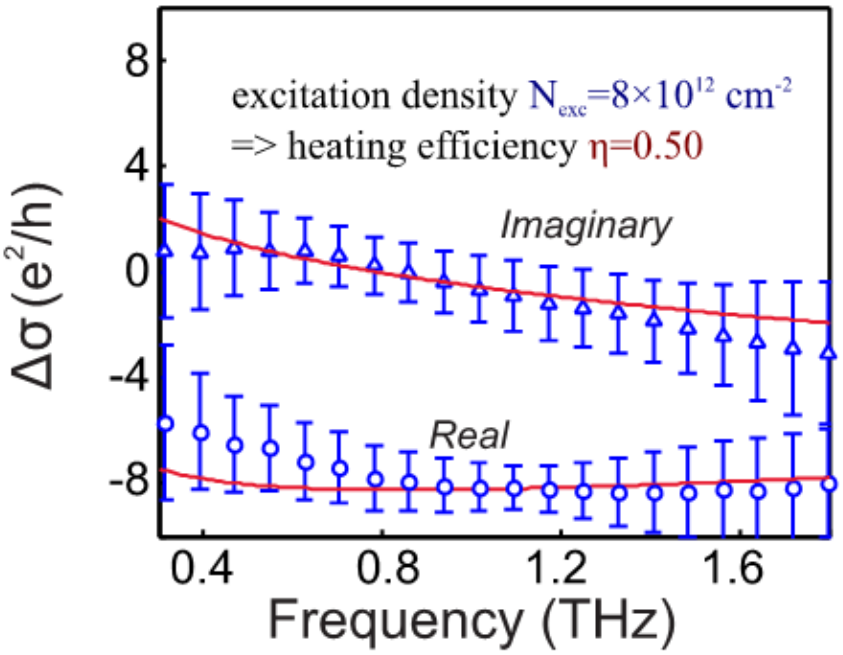

Fig. 4 Measured (symbols) and fitted (lines) THz photoconductivity spectra of doped graphene, photo-excited at 800 *nm*, leading to photo-carrier density of 8×10^{12} cm^{-2}.

From the extracted effective carrier temperature, which is a fit parameter in Fig. 4, one readily obtains the total thermal energy of electron gas in graphene ΔQ. Comparison of this electron heat with the total energy of photoexcitation E_{phot} yields the heating efficiency $\eta = \Delta Q/E_{\text{phot}}$, which for the case shown in Fig. 4 equals $\eta \approx 0.5$. That is about 50% of optical excitation energy which was directly converted in the electron heat via electron-electron interaction process, while the rest of the energy of the photo-excited (i.e. high-energy) carriers was used on interaction with the lattice via phonon emission [29].

It is interesting to quantify the trend in the split ratio between the optical excitation energy converted into electron heat, and that directly spent on excitation of the lattice. In Fig. 5 we present the dependency of electron heating efficiency via optical excitation as function of

photoexcited carrier density. At weaker excitation almost 100% of photon energy is converted into electron heat, whereas with increase in the photocarrier density the heating efficiency tends to the values $\eta \approx 0.5$ [29]. Such a behavior can be well understood qualitatively: if the total excess energy delivered by optical excitation is small, the background free carrier population will absorb it with very high efficiency via ultrafast electron-electron interaction. However, if the excess energy becomes large, the competing, yet slower, energy dissipation channel - the phonon emission – becomes activated and increases in its importance [29].

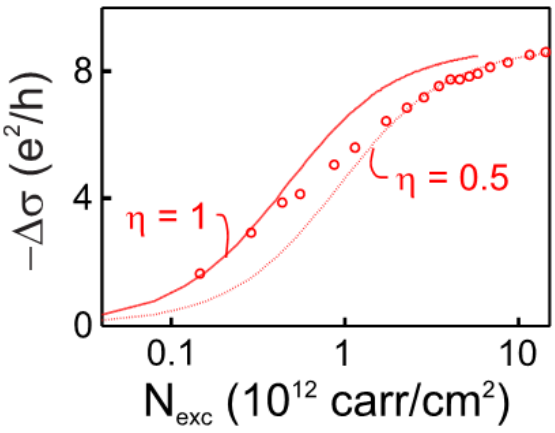

Fig. 5 Measured (symbols) and fitted (lines) THz photoconductivity spectra of doped graphene, photo-excited at 800 *nm*, leading to photo-carrier density of 8×10^{12} cm^{-2}.

We note, that in patterned graphene – such as e.g. controllably-folded graphene (GraFold), where the background doping is spatially-anisotropic, the negative photoconductivity, which is realted to carrier heating efficiency via optical excitation, also shows a sizeable spatial anisotropy which can be as high as 1.4:1 [33].

6. Ultrafast photoconductivity of graphene nanostructures – graphene nanoribbons and carbon nanotubes.

Electron conduction in graphene nanostructures is radically different from that of graphene. In graphene the bandgap is zero, and the energy-momentum dispersion is linear $E = pv_F$, which means the electrons behave as massless particles with the constant (ballistic) group velocity v_F. In graphene nanostructures such as graphene nanoribbons (GNRs) and carbon nanotubes (CNTs) quantum confinement opens up the bandgap, which leads to the deviation of energy-momentum dispersion from linear dependency. As a result, the carriers acquire massive properties, as the electronic states around the bandgap can be described by an effective dispersion $E = p^2/2m^*$, where m^* is a non-zero effective mass. Massive nature makes the carriers in graphene nanostructure subject to Coulomb binding effects, such as exciton formation and trapping onto the charged impurities. As a result, the transport in graphene nanostructures closely resembles

that of organic semiconductors, with positive photoconductivity, and very strong exciton effect.

In Fig. 6 we show the THz frequency-integrated photoconductivity dynamics in the suspension of semiconducting single-wall CNTs (SW-CNTs) with the diameter D = 0.76 *nm*, photoexcited at 400 *nm* [34]. The bandgap energy of the CNTs is around 1.9 *eV*. The photoconductivity of SW-CNTs is positive and very short-lived. We have also studied the dynamics of the photoconductivity of atomically-precise GNRs [35] with similar dimensions and similar bandgap energy, and found it to be very similar to that of the CNTs shown in Fig. 6.

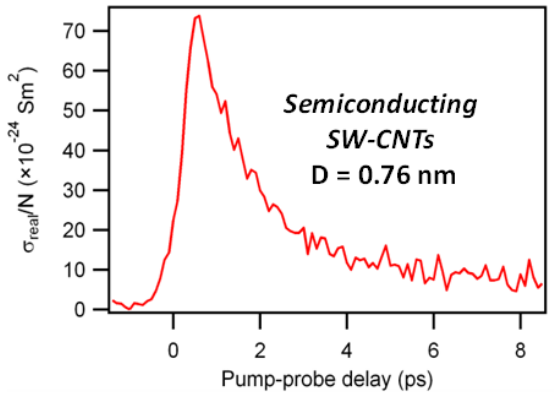

Fig. 6 Transient THz photoconductivity of semiconducting single-wall CNTs suspended in gel, photoexcited at 400 *nm*. The CNT diameter is D = 0.76 *nm*.

The frequency-resolved optical pump-THz probe spectroscopy allows us to elucidate the nature of conduction in graphene nanostructures. The photoconductivity of both CNTs and GNRs, as shown in Fig. 7, has been found to be governed by the free charge, experiencing the long-range localization and strong electron momentum backscattering [34]. Such a conduction is well-described by the Drude-Smith model [36], and is typical for most organic semiconductors [37] [38].

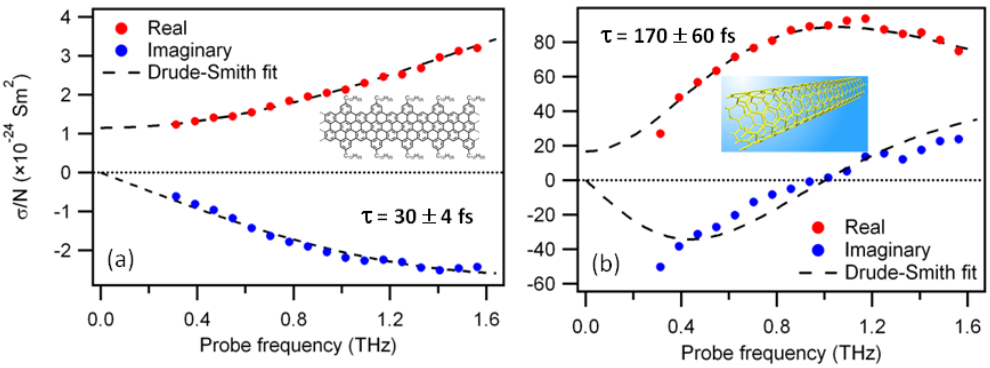

Fig. 7 THz photoconductivity of (a) GNRs and (b) CNTs, normalized to absorbed photon density (photoexcitation wavelength of 400 *nm*). Solid lines - Drude-Smith fits. Extracted electron momentum scattering times are shown in insets.

The Drude-Smith fits to measure THz photoconductivity under 400 *nm* photoexcitation yielded, in particular, significantly different momentum scattering times for conduction electrons, 30 ±4 *fs* for GNRs, as compared to 170 ±60 *fs* for CNTs. Considerably longer ballistic transport times for electrons in CNTs can be explained by higher structural rigidity of this type of 1D graphene nanostructure, as compared to GNRs [34]. Indeed, it is reasonable to expect a smaller density of twist and bend defects in the CNTs than in GNRs. The free-carrier quantum yield of 3 – 30% for graphene nanostructures points to a strong exciton effect, precisely as expected from the strongly-confined structures with massive electrons and holes subject to Coulomb effects.

7. Conclusions.

We have presented a comprehensive picture of ultrafast THz carrier dynamics in graphene and graphene nanostructures. In graphene, where the carriers behave as massless Dirac fermions, the intrinsic and photo-conductivity in the THz range is governed by the thermodynamic balance maintained within the electron population in graphene, which acts as a thermalized electrons gas. The extremely efficient, near-instantaneous electron heating in graphene, compared to the considerably slower cooling via phonon emission can be well exploited technologically. Since this leads to a significant high-energy electron population in THz-irradiated graphene, this can be used for efficient room-temperature THz photo-thermoelectric detectors. Indeed, very recent successful demonstration of such devices [39, 40] based on both the CVD and exfoliated graphene, as well as an efficient hot-carrier extraction from graphene into the external circuit [41], are promising steps towards practical application of hot-carrier electronics in graphene. The results of this work, including our simple thermodynamic model of THz interaction with doped single-layer graphene [14], may be directly applied to understanding and optimization of graphene-based electronics operating in strongly nonequilibrium regime. The performance of devices such as high-speed MOSFETs [1, 23], room-temperature THz detectors [39, 40] potentially leading to inexpensive and efficient graphene-based THz imaging cameras, or THz-bandwidth detectors for ultra-high-speed THz-wave wireless communications [42] can be thus adequately predicted and optimized.

In graphene nanostructures, on the other hand, the opening of the bandgap provides for the massive nature of electrons and holes. As a result, the of GNRs and CNTs is governed by the free massive carriers experiencing the long-range localization, well described by the Drude-Smith conductivity model. The high structural rigidity of CNTs results in a considerably high photoconductivity with the ballistic electron transport times as long as ~ 170 *fs*, which has a clear technological potential.

Acknowledgments.

D. T. acknowledges the EU Career Integration Grant 334324 (LIGHTER). K. J. T.

acknowledges support from an NWO Rubicon grant. F. K. acknowledges support by the Fundacio Cellex Barcelona, the EU Career Integration Grant 294056 (GRANOP), the ERC Starting Grant 307806 (CarbonLight), and support by the EC under Graphene Flagship (No. CNECT-ICT-604391). X. F. and K. M. acknowledge ERC grants on NANOGRAPH and 2DMATER, DFG Priority Program SPP 1459, EU Project GENIUS, MOLESOL, and EC under Graphene Flagship (No. CNECT-ICT-604391).

References:

1. F. Schwierz. "Graphene transistors". *Nat. Nanotechnol*. 5, 487–496 (2010).

2. K. S. Novoselov, A. K. Geim, S. V Morozov, et al. "Two-dimensional gas of massless Dirac fermions in graphene". *Nature* 438, 197–200 (2005).

3. K. S. Novoselov, A. K. Geim, S. V Morozov, et al. "Electric field effect in atomically thin carbon films". *Science* 306, 666–669 (2004).

4. C. Berger, Z. Song, T. Li, et al. "Ultrathin epitaxial graphite : 2D electron gas properties and a route toward graphene-based nanoelectronics". *J. Phys. Chem*. B 108, 19912–19916 (2004).

5. R. Cheng, J. Bai, L. Liao, et al. "High-frequency self-aligned graphene transistors with transferred gate stacks". *Proc. Natl. Acad. Sci*. U. S. A. 109, 11588–11592 (2012).

6. X. Li, W. Cai, J. An, et al. "Large-area synthesis of high-quality and uniform graphene films on copper foils". *Science* 324, 1312–1314 (2009).

7. S. Ryu, L. Liu, S. Berciaud, et al. "Atmospheric oxygen binding and hole doping in deformed graphene on a SiO2 substrate". *Nano Lett*. 10, 4944–4951 (2010).

8. G. Jnawali, Y. Rao, H. Yan, et al. "Observation of a transient decrease in terahertz conductivity of single-layer graphene induced by ultrafast optical excitation". *Nano Lett*. 13, 524–530 (2013).

9. A. C. Ferrari, J. C. Meyer, V. Scardaci, et al. "Raman spectrum of graphene and graphene layers". *Phys. Rev. Lett*. 97, 187401 (2006).

10. A. C. Ferrari. "Raman spectroscopy of graphene and graphite: Disorder, electron–phonon coupling, doping and nonadiabatic effects". *Solid State Commun*. 143, 47–57 (2007).

11. Y. Hao, M. S. Bharathi, L. Wang, et al. "The role of surface oxygen in the growth of large single-crystal graphene on copper". *Science* 342, 720–723 (2013).

12. S. Tani, F. Blanchard, and K. Tanaka. "Ultrafast carrier dynamics in graphene under a high electric field". *Phys. Rev. Lett*. 109, 166603 (2012).

13. H. Y. Hwang, N. C. Brandt, H. Farhat, et al. "Nonlinear THz conductivity dynamics in P-type CVD-grown graphene". *J. Phys. Chem*. B 117, 15819–15824 (2013).

14. Z. Mics, K.-J. Tielrooij, K. Parvez, et al. "Thermodynamic picture of ultrafast charge transport transport in graphene". *Nat. Commun*. DOI: 10.1038/ncomms8655 (2015).

15. T. Kampfrath, K. Tanaka, and K. A. Nelson. "Resonant and nonresonant control over matter and light by intense terahertz transients". *Nat. Photonics* 7, 680–690 (2013).

16. R. Ulbricht, E. Hendry, J. Shan, et al. "Carrier dynamics in semiconductors studied with time-resolved terahertz spectroscopy". *Rev. Mod. Phys*. 83, 543–586 (2011).

17. K.-L. Yeh, M. C. Hoffmann, J. Hebling, et al. "Generation of 10 \mu J ultrashort terahertz pulses by optical rectification". *Appl. Phys. Lett.* 90, 171121 (2007).

18. H. Hirori, A. Doi, F. Blanchard, et al. "Single-cycle terahertz pulses with amplitudes exceeding 1 MV/cm generated by optical rectification in LiNbO3". *Appl. Phys. Lett.* 98, 091106 (2011).

19. M. J. Paul, Y. C. Chang, Z. J. Thompson, et al. "High-field terahertz response of graphene". *New J. Phys*. 15, 085019 (2013).

20. M. C. Hoffmann and D. Turchinovich. "Semiconductor saturable absorbers for ultrafast terahertz signals". *Appl. Phys. Lett*. 96, 151110 (2010).

21. F. Blanchard, D. Golde, F. Su, L. Razzari, et al. "Effective mass anisotropy of hot electrons in nonparabolic conduction bands of n-doped InGaAs films using ultrafast terahertz pump-probe techniques". *Phys. Rev. Lett*. 107, 107401 (2011).

22. D. Turchinovich, J. M. Hvam, and M. C. Hoffmann. "Self-phase modulation of a single-cycle terahertz pulse by nonlinear free-carrier response in a semiconductor". *Phys. Rev.* B 85, 201304 (2012).

23. F. Schwierz. "Graphene transistors: status, prospects, and problems". *Proc. IEEE* 101, 1567–1584 (2013).

24. R. R. Nair, P. Blake, A. N. Grigorenko, et al."Fine structure constant defines visual transparency of graphene". *Science* 320, 1308 (2008).

25. K. J. Tielrooij, J. C. W. Song, S. A. Jensen, et al. "Photoexcitation cascade and multiple hot-carrier generation in graphene". *Nat. Phys.* 9, 248–252 (2013).

26. J. C. W. Song, K. J. Tielrooij, F. H. L. Koppens, et al. "Photoexcited carrier dynamics and impact-excitation cascade in graphene". *Phys. Rev*. B 87, 155429 (2013).

27. J. C. Johannsen, S. Ulstrup, F. Cilento, et al. "Direct view of hot carrier dynamics in graphene". *Phys. Rev. Lett.* 111, 027403 (2013).

28. I. Gierz, J. C. Petersen, M. Mitrano, et al. "Snapshots of non-equilibrium Dirac carrier distributions in graphene". *Nat. Mater*. 12, 1119–1124 (2013).

29. S. A. Jensen, Z. Mics, I. Ivanov, et al. "Competing ultrafast energy relaxation pathways in photoexcited graphene". *Nano Lett*. 14, 5839 – 5845 (2014).

30. S. Das Sarma, S. Adam, E. H. Hwang, et al. "Electronic transport in two-dimensional graphene". *Rev. Mod. Phys.* 83, 407–470 (2011).

31. N. W. Ashcroft and N. D. Mermin. *Solid State Physics* (Brooks/Cole, 1976).

32. A. H. Castro Neto, F. Guinea, N. M. R. Peres, et al. "The electronic properties of graphene". *Rev. Mod. Phys.* 81, 109–162 (2009).

33. T. Hallam, A. Shakouri, E. Poliani, et al. "Controlled folding of Graphene: GraFold Printing". *Nano Lett.* 15, 857 – 863 (2014).

34. S. A. Jensen, R. Ulbricht, A. Narita, et al. "Ultrafast Photoconductivity of Graphene Nanoribbons and Carbon Nanotubes". *Nano Lett.* 13, 5925 – 5930 (2013).

35. A. Narita, X. Feng, Y. Hernandez, et al. "Synthesis of structurally well-defined and liquid-phase-processable graphene nanoribbons". *Nat. Chem*. 6, 126–32 (2014).

36. N. Smith. "Classical generalization of the Drude formula for the optical conductivity". *Phys. Rev*. B 64, 155106 (2001).

37. E. Hendry, J. Schins, L. Candeias, et al. "Efficiency of Exciton and Charge Carrier Photogeneration in a Semiconducting Polymer". *Phys. Rev. Lett.* 92, 196601 (2004).

38. Z. Jin, D. Gehrig, C. Dyer-Smith, et al. "Ultrafast Terahertz Photoconductivity of Photovoltaic Polymer − Fullerene Blends: A Comparative Study Correlated with Photovoltaic Device Performance". *J. Phys. Chem. Lett*. 5, 3662–3668 (2014).

39. M. Mittendorff, S. Winnerl, J. Kamann, et al. "Ultrafast graphene-based broadband THz detector". *Appl. Phys. Lett.* 103, 021113 (2013).

40. X. Cai, A. B. Sushkov, R. J. Suess, et al. "Sensitive room-temperature terahertz detection via the photothermoelectric effect in graphene". *Nat. Nanotechnol*. 9, 814 – 819 (2014).

41. N. M. Gabor, J. C. W. Song, Q. Ma, et al. "Hot carrier-assisted intrinsic photoresponse in graphene". *Science* 334, 648–652 (2011).

42. M. C. Hoffmann, B. S. Monozon, D. Livshits, et al. "Terahertz electro-absorption effect enabling femtosecond all-optical switching in semiconductor quantum dots". *Appl. Phys. Lett*. 97, 231108 (2010).